

PAPER View Article Online
View Journal | View Issue



Cite this: Phys. Chem. Chem. Phys., 2016, **18**, 17646

Received 21st February 2016, Accepted 3rd June 2016

DOI: 10.1039/c6cp01183g

www.rsc.org/pccp

# Mechanism of X-ray excited optical luminescence (XEOL) in europium doped BaAl<sub>2</sub>O<sub>4</sub> phosphor

Marcos V. dos S. Rezende,\* Paulo J. R. Montes, Adriano B. Andrade, Zelia S. Macedo and Mário E. G. Valerio de Adriano B. Andrade,

This paper reports a luminescence mechanism in Eu-doped  $BaAl_2O_4$  excited with monochromatic X-rays (also known as X-ray excited optical luminescence – XEOL) from synchrotron radiation. The material was prepared *via* a proteic sol–gel methodology. The X-ray absorption near edge structures (XANES) at the Ba  $L_{III}$ - and Eu  $L_{III}$ -edges exhibit typical absorption spectra. XEOL spectra recorded in energy ranges, either around the Ba  $L_{III}$ - or Eu  $L_{III}$ -edges, showed important differences concerning the intensity of the Eu<sup>2+</sup> or Eu<sup>3+</sup> emission bands. Nevertheless, the total area under the XEOL spectra increases as the energy of the X-ray photons increases in both ranges (Ba  $L_{III}$ - and Eu  $L_{III}$ -edges).

## 1 Introduction

The research and development of new scintillator materials is a field that experienced a fast increase in the last decade and the search for faster and more efficient materials was always the main focus of all research in this area. Scintillation is a kind of radioluminescence (RL) phenomenon where the absorption of high-energy photons or energetic particle beams leads to an observable light emission. Scintillators can be used for medical imaging using X-rays and gamma rays, geophysical exploration, and numerous other scientific and industrial applications.<sup>1</sup>

Rare-earth (RE) ions are the most widely used activators for the modification of fluoride and oxide scintillator materials. In general, cerium, ytterbium and europium are the commonly used activators. The europium and cerium activated crystals, in particular, have received considerable attention because of the 5d  $\rightarrow$  4f allowed transition of trivalent cerium (Ce<sup>3+</sup>) and divalent europium (Eu<sup>2+</sup>), good light yield and energy resolution achieved in several dense materials.<sup>2,3</sup>

At the present time, several single-crystal scintillators are used. For example, fluoride based materials like pure CaF<sub>2</sub><sup>2</sup> and CaF<sub>2</sub>:Eu,<sup>4</sup> LiCaAlF<sub>6</sub>:Eu and LiCaAlF<sub>6</sub>:Ce,<sup>5</sup> and the oxide scintillators, such as LuAlO<sub>3</sub>:Ce,<sup>6</sup> YAlO<sub>3</sub><sup>7</sup> and BGO.<sup>8</sup> SrAl<sub>2</sub>O<sub>4</sub>:Eu was recently

Recently, BaAl<sub>2</sub>O<sub>4</sub> doped with other rare-earth ions has been investigated due to its several optical properties. Most recently optical properties observed in BaAl<sub>2</sub>O<sub>4</sub> were the long lasting phosphorescence (LLP), which is activated by the presence of rare earth ions. Sakai et al. 10 and Qiu et al. 11 reported LLP in BaAl<sub>2</sub>O<sub>4</sub>:Eu<sup>2+</sup>,Dy<sup>3+</sup> and BaAl<sub>2</sub>O<sub>4</sub>:Eu<sup>2+</sup>,Nd<sup>3+</sup>, respectively. On the other hand, Jia et al. 12 reported long afterglow observed by the eye in darkness for as long as 10 h in BaAl<sub>2</sub>O<sub>4</sub>:Ce<sup>3+</sup> and BaAl<sub>2</sub>O<sub>4</sub>:Ce<sup>3+</sup>,Dy<sup>3+</sup>. The photoluminescence properties were also observed in Tm<sup>3+</sup>- and Tb<sup>3+</sup>-doped BaAl<sub>2</sub>O<sub>4</sub>. <sup>13</sup> This material is derived from the structure of SiO<sub>2</sub> b-tridymite and exhibit two hexagonal phases with a reversible transition at 123 °C. The ferroelectric phase with the space group  $P6_3$  is stable at room temperature while the paraelectric phase with the space group P6<sub>3</sub>22 is observed at high temperatures. At room temperature, the P63 phase of BaAl2O4 is composed of two different barium sites, Ba1 and Ba2, which are positioned on Wyckoff positions 6c and 2a, respectively, coordinated by nine oxygen ions and there are four types of Al<sup>3+</sup> in [AlO<sub>4</sub>] tetrahedra.

XEOL is the optical luminescence emitted when the core-level X-ray excitation occurs. This phenomenon can be used as a mode for X-ray absorption fine structure (XAFS). XEOL detection techniques may offer additional capabilities to XAFS spectroscopy, and may contain information that is not obtainable by other experimental techniques. For example, it may be possible to obtain information about the local structure of only the atom involved in the luminescence emission (site-specific). Site selectivity would offer an enormous advantage for XAFS studies

proven to be a good candidate exhibiting interesting radioluminescence properties when excited with X-rays. BaAl<sub>2</sub>O<sub>4</sub>:Eu belongs to the same family of aluminates such as SrAl<sub>2</sub>O<sub>4</sub> with the advantage of having a higher electronic density due to the presence of Ba<sup>2+</sup> ions in place of Sr<sup>2+</sup>.

<sup>&</sup>lt;sup>a</sup> Grupo de Nanomateriais Funcionais (GNF), Departamento de Física, Universidade Federal de Sergipe, Campus Universitário Professor Alberto Carvalho, 49500-000 Itabaiana-SE, Brasil. E-mail: mvsrezende@gmail.com; Tel: +55-(79)3432-8225

<sup>&</sup>lt;sup>b</sup> Coordenadoria de Física, Instituto Federal de Sergipe, 49400-000, Lagarto-SE, Brasil

<sup>&</sup>lt;sup>c</sup> Laboratório de Preparação e Caracterização de Materiais, Departamento de Física, Universidade Federal de Sergipe, Campus Universitário Professor José Aloísio de Campos, 49100-000, São Cristovão-SE, Brasil

<sup>&</sup>lt;sup>d</sup> Programa de Pós-Graduação em Ciências e Engenharia de Materiais, Universidade Federal de Sergipe, 49100-000, São Cristovão-SE, Brasil

involving a wide range of problems, notably environmental and other multicomponent samples that are not able to be studied with more conventional structural techniques.<sup>15</sup>

The study of luminescence spectrum, measured as a function of X-ray energy, was first reported by Bianconi et al. 16 in CaF<sub>2</sub> as the X-ray energy was scanned over a region that included the Ca K-absorption edge. They found a negative jump in the XEOL-XAS, i.e., a decrease, rather than an increase as observed in the XAS at the Ca K-absorption edge. The observed luminescence was attributed to the recombination of the self-trapped excitons (STEs) created by the excitation of Ca core electrons into the continuum. On the other hand, Goulon et al. 17 found a positive edge jump in the XEOL-XAS in several other luminescent materials. It was also found that the sign of the edge jump is strongly dependent on the sample and on whether a "backscattering" (R) or a "transmission" (T) geometry measure was used. Based on this information, Goulon et al. 17 proposed a phenomenological model that could accommodate positive or negative edge jumps depending on the sample properties and on the selected geometrical arrangement. The predictions were found to be consistent with numerous experimental spectra. Nevertheless, the predictions remained unclear for a single crystal whereas XEOL-XAS exhibited a negative edge jump. 18 Emura et al. 19 proposed another phenomenological model relying essentially on more parameters. They even proposed to introduce specific excitation yields for each atom of the luminescent crystalline matrix.

Published studies on XEOL have mainly focused on understanding the intensity of the luminescence response that occurs as the excitation energy is scanned through a core absorption edge. Therefore, in the present work, XEOL is used for the first time to study BaAl<sub>2</sub>O<sub>4</sub>:Eu prepared via a new proteic sol-gel method. Monochromatic X-rays from synchrotron radiation tuned at the Ba L<sub>III</sub>-edge and at the Eu L<sub>III</sub>-edge was used. Both the XAS and the total XEOL-XAS light yield were recorded as a function of the incident X-ray photon energy. Simultaneously, the usual EXAFS and XANES measurements were performed and compared to the XEOL results. This combination of experimental techniques allowed us to propose a mechanism that involves the emission of Eu<sup>2+</sup> and Eu<sup>3+</sup> ions in the XEOL spectra during irradiation with X-rays and explain that Eu oxidation states depend on the excitation energies. In the proposed mechanism it was possible to connect direct or inverted absorption edges with the de-excitation process. We obtained a set of rate equations that describe the traffic of charge carriers involved in the emission of Eu2+ and Eu3+ ions when the sample is excited around the Ba L<sub>III</sub>-edge.

## 2 Experimental

Nanopowder samples of BaAl2O4 and Ba0.97Eu0.03Al2O4 were prepared via a proteic sol-gel route.15 This methodology has been used routinely in our laboratory to produce a number of different oxide materials<sup>20</sup> and it has already been applied to produce other aluminate compounds, for example SrAl<sub>2</sub>O<sub>4</sub>.9

In the first step, Ba(NO<sub>3</sub>)<sub>2</sub> and Al(NO<sub>3</sub>)<sub>3</sub>9H<sub>2</sub>O salts were mixed with coconut water (Cocos nucifera) forming the starting gel. For the doped samples, 0.97 mol of Ba(NO<sub>3</sub>)<sub>2</sub>, 0.03 mol of EuCl<sub>3</sub>6H<sub>2</sub>O and 1 mol of Al(NO<sub>3</sub>)<sub>3</sub>9H<sub>2</sub>O were used. In the second step, the gel was dried at 100 °C for 24 h, forming a xerogel. In the last step, the xerogel was calcined at 1100 °C for 2 h in air.

The crystalline phases were identified by powder X-ray diffraction (XRD) measurements using a Rigaku Ultima + RINT 2000/PC diffractometer in the Bragg-Brentano geometry, using Cu Kα radiation, operating at 40 kV and 40 mA. The X-ray diffraction patterns were compared with those obtained in the previous study.21 The X-ray absorption spectroscopy (XAS) measurements were performed around the Ba LIII and Eu LIII absorption edges in the X-ray absorption fine structure - XAFS-2 beamline at LNLS (Brazilian Synchrotron Light Laboratory, Campinas, Brazil). The XEOL excitation and emission spectra were measured simultaneously using a Hamamatsu R928Q PMT and an Ocean Optics HR2000 spectrometer connected to a bifurcated optical fiber that collected the light generated during the XEOL measurements sending it to the PMT and the spectrometer. All measurements were performed at room temperature.

## 3 Results

Fig. 1 and 2 show the XEOL spectra of the Eu<sup>3+</sup> doped sample when excited around the Ba  $L_{III}$  (see Fig. 1) and Eu  $L_{III}$  (see Fig. 2) edges.

The XEOL spectra are quite different from the photoluminescence (PL) emission spectra of BaAl<sub>2</sub>O<sub>4</sub>:Eu<sup>3+</sup> shown in previous work.<sup>22</sup> PL spectra show typical emission peaks from Eu<sup>3+</sup> observed in the range of 550–750 nm. These are assigned to the transitions of  ${}^5D_0 \rightarrow {}^7F_I (J = 0 \text{ to } 4)$  states. The emission spectra recorded when the sample is excited with UV-visible light (PL) are different from the emission spectra recorded when excited with ionizing radiation (XEOL). The broad band between 350 and 550 nm is characteristic of the Eu<sup>2+</sup> emission, due to  $4f5d \rightarrow 4f$  transitions.

The broad band of the Eu<sup>2+</sup> emission could be separated into two Gaussians with the maxima at about 451 and 508 nm,

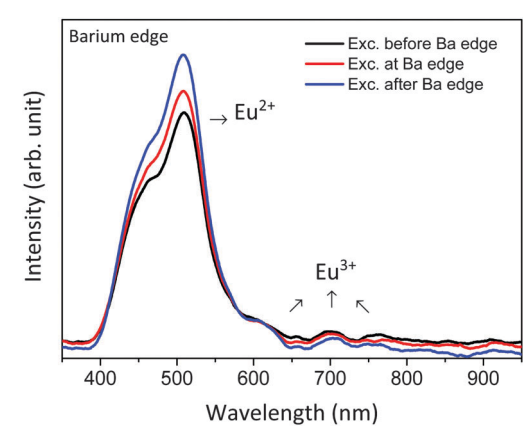


Fig. 1 XEOL emission spectra of BaAl<sub>2</sub>O<sub>4</sub>:Eu<sup>2+</sup> excited before, after and at

Europium edge

Exc. before Eu edge
lifetii

mo)

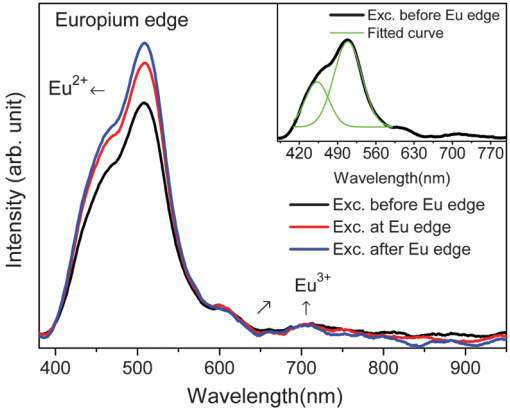


Fig. 2 XEOL emission spectra of  $BaAl_2O_4$ :  $Eu^{2+}$  excited at before, after and at the Eu  $L_{iii}$  edge.

respectively (see inset in Fig. 2). When the local symmetry of the  $\mathrm{Eu^{2^+}}$ -dopant in the matrix is unique, only one intense peak is expected. On the other hand, if the matrix has two or more non-symmetric  $\mathrm{Eu^{2^+}}$ -possible sites, the number of bands will reflect these multiple symmetric sites. This effect is explained by the splitting of the 5d-excitation level of  $\mathrm{Eu^{2^+}}$  that occurs due to the strong influence of the crystal field. Since each of the non-equivalent  $\mathrm{Eu^{2^+}}$  sites presents a different local symmetry, they will have a different crystal field splitting giving rise to more than one band in the emission spectra associated with the 4f5d  $\rightarrow$  4f transition. This is the case in BaAl<sub>2</sub>O<sub>4</sub>, where two non-equivalent  $\mathrm{Ba^{2^+}}$  sites are available for the  $\mathrm{Eu^{2^+}}$  ions.

In general, substitution might occur at either the  $Ba^{2^+}$  or  $Al^{3^+}$  site, and there is more than one possible mode of charge compensation when needed. Previous theoretical work<sup>23</sup> in  $BaAl_2O_4$  shows that  $Eu^{2^+}$  ions can be incorporated into two non-equivalent barium sites due to the similar ionic radii of  $Eu^{2^+}$  (1.44 Å) and  $Ba^{2^+}$  (1.47 Å)<sup>24</sup> and equal oxidation states. Thus, the shoulder observed in the curves of Fig. 1 and 2 is due to the incorporation of  $Eu^{2^+}$  into two different sites, in agreement with the results observed in computational study.<sup>23</sup>

The intense peak observed at around 500 nm is consistent with that observed at 500 nm reported by Sakai et~al.,  $^{10}$  at 496 nm reported by Lin et~al.,  $^{25}$  and at 505 nm found by Palilla et~al.  $^{26}$  and Blasse et~al.  $^{27}$  in BaAl<sub>2</sub>O<sub>4</sub>. Peng et~al.  $^{28}$  also reported two intense peaks at around 500 nm in BaAl<sub>2</sub>O<sub>4</sub>, the first one at 495 nm and the second one at 530 nm. The small difference in the wavelengths between Peng's work and the present work might be due to the way that Eu<sup>2+</sup> was produced in the BaAl<sub>2</sub>O<sub>4</sub> matrix. In the work of Peng et~al.,  $^{28}$  the reduction of Eu<sup>3+</sup>  $\rightarrow$  Eu<sup>2+</sup> occurred during the calcination step and the dopant dissolved in the crystalline matrix already in the divalent oxidation state. Conversely, in the present work, the Eu<sup>3+</sup> reduction process occurs due to the X-ray excitation after absorbing X-rays.

Additionally in Fig. 1 and 2, one can see weaker peaks at about 612 nm and 700 nm associated with the  $^5D_0 \rightarrow ^7F_2$  and  $^5D_0 \rightarrow ^7F_4$  transitions of Eu<sup>3+</sup>. The weak emission intensity of the 4f  $\rightarrow$  4f transitions of Eu<sup>3+</sup> may be due to the difference in lifetime transition of Eu<sup>2+</sup> and Eu<sup>3+</sup> ions. The Eu<sup>2+</sup> ions,

whose 4f<sup>6</sup>5d<sup>1</sup>-4f<sup>7</sup> transitions are allowed, have a much shorter lifetime (ca. 1 ms) than the 4f  $\rightarrow$  4f transitions of Eu<sup>3+</sup> (several ms) and thus a larger transition probability. This means that X-ray irradiation is not able to reduce all Eu<sup>3+</sup> to Eu<sup>2+</sup>. The coexistence of both valences of Eu is also confirmed by the XANES result discussed below. The broad Eu3+ emission is connected to inhomogeneous broadening. Small differences in the site symmetry slightly change the energy levels of the dopant changing the emission energy of Eu<sup>3+</sup> ions. This inhomogeneous broadening is a result of crystal inhomogeneity causing small distortions around europium ions.<sup>29</sup> In the BaAl<sub>2</sub>O<sub>4</sub> structure, Eu<sup>3+</sup> ions are preferably placed at the Ba site with charge compensation by interstitial oxygen (one interstitial compensating 2 europium ions).<sup>21</sup> Therefore, three factors can contribute to the local disorder (crystal inhomogeneity): the ionic radii difference between europium and barium sites, two Eu<sup>3+</sup> ions with different local symmetry and charge compensation close to europium ions, which can change the local environment. The RL emission of Eu-doped SrAl<sub>2</sub>O<sub>4</sub> reported by Montes et al.30 also exhibits an intense broad peak at about 515 nm associated with Eu<sup>2+</sup> 5d4f  $\rightarrow$  4f transitions and the presence of a less intense and sharp peak at about 612 nm, associated with the Eu<sup>3+ 5</sup>D<sub>0</sub>  $\rightarrow$  <sup>7</sup>F<sub>2</sub> transition.

The total XEOL yield and the conventional XAS data are shown in Fig. 3 and 4. The XAS and XEOL excitation spectra of the measurements were both normalized by the initial intensity of the radiation beam  $(I_0)$  and measured simultaneously. In Fig. 3 the Eu<sup>3+</sup> doped sample was measured in the X-ray energies around the Ba  $L_{\rm III}$ -edge. The XAS curve showed a typical X-ray absorption edge response to  $Ba^{2+}$  ions. The intensity of the XEOL-XAS spectrum increases as the photon energy increases in this range.

Fig. 4 presents the emission spectra of the sample excited with X-ray photon energies around the Eu  $L_{\rm III}$ -edge and the usual X-ray absorption spectra measured in X-ray transmission mode. The XANES measurement of the Eu  $L_{\rm III}$ -edge shows two typical lines. The first at 6974 eV is due to the presence of Eu<sup>2+</sup> in the samples. The second at 6983 eV is due to the Eu<sup>3+</sup> ions. Such results corroborate the results previously shown in Fig. 2,

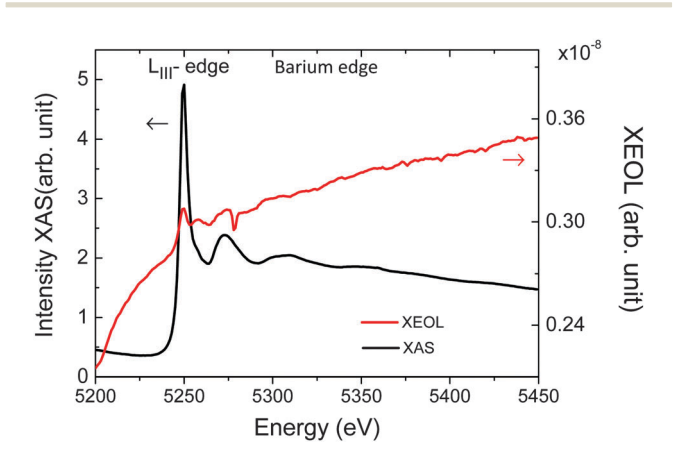


Fig. 3 XAS and XEOL curves of  $BaAl_2O_4$ :Eu excited near  $Ba\ L_{III}$  edges (XANES).

**PCCP Paper** 

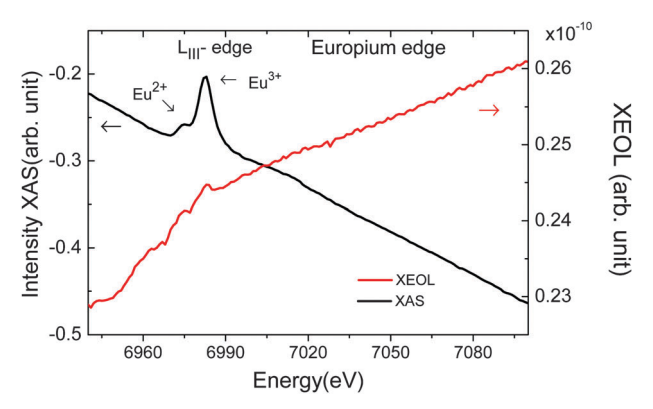


Fig. 4 XAS and XEOL curves of BaAl<sub>2</sub>O<sub>4</sub>:Eu excited in the region of Eu L<sub>III</sub> edges.

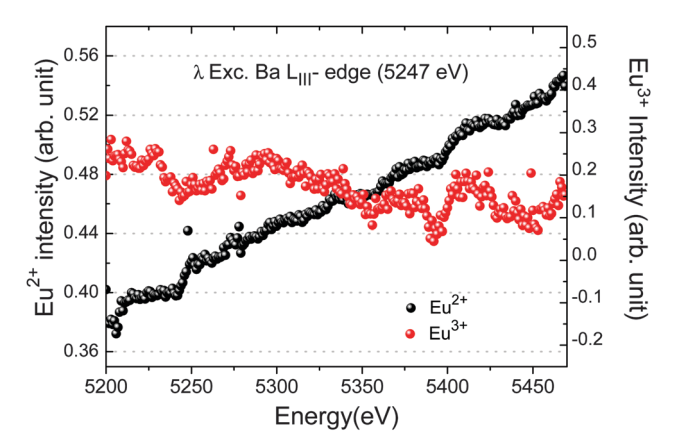


Fig. 5 Eu<sup>2+</sup> and Eu<sup>3+</sup> XEOL intensity emission of the bands as a function of the incident photon energy around the Ba  $L_{\rm III}$  edge

where the reduction process of part of the original  $Eu^{3+} \rightarrow Eu^{2+}$ occurs when the sample is excited with X-rays. In Fig. 4, it is also observed that the intensity of XEOL-XAS increases as the energy of the incident photons increases. This behavior is similar to the one observed in SrAl<sub>2</sub>O<sub>4</sub>:Eu by Montes et al.<sup>31</sup>

The full XEOL spectrum measured as a function of the incident X-ray photon energy contributed to the identification of the trends of each emission band. The Eu<sup>2+</sup> and Eu<sup>3+</sup> intensity emission can be separated from the full XEOL emission by computing separately the areas under the Eu<sup>2+</sup> and the Eu<sup>3+</sup> emission bands for each excitation energy. The results of these analyses are shown in Fig. 5 and 6, where these separated areas under the Eu<sup>2+</sup> or Eu<sup>3+</sup> emission were plotted as a function of the X-ray energy around the Ba  $L_{\rm III}$  edge and the Eu  $L_{\rm III}$  edge respectively. It is possible to see that the Eu<sup>2+</sup> emission increased for both cases while the Eu3+ decreased for both the excitation energies, but the decrease rate for the energies around the Eu L<sub>III</sub> edge is very small.

#### Discussion

The main results can be summarized as follows: (i) Eu is incorporated in the BaAl<sub>2</sub>O<sub>4</sub> matrix as a trivalent ion; (ii) both

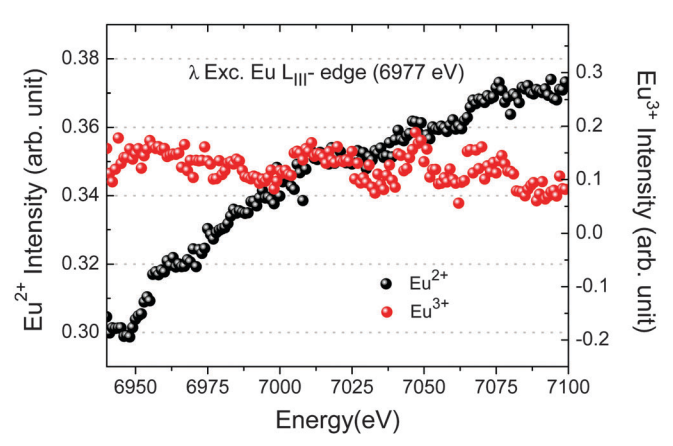


Fig. 6 Eu<sup>2+</sup> and Eu<sup>3+</sup> XEOL intensity emission of the bands as a function of the incident photon energy around the Eu L<sub>III</sub> edge.

Eu<sup>3+</sup> and Eu<sup>2+</sup> are located in two non-equivalent sites; (iii) irradiation with X-rays reduces a great amount of Eu3+ to Eu<sup>2+</sup>; (iv) during irradiation typical Eu<sup>2+</sup> and Eu<sup>3+</sup> emissions were observed with their intensities depending on the incident photon energy: while the Eu<sup>2+</sup> XEOL emission always increases as the X-ray energy increases, the Eu<sup>3+</sup> XEOL emission intensity decreases and these behaviours are the same for both energy ranges studied, around the Ba LIII edge or the Eu LIII edge.

Two main questions arise from these results: (1) What is the process that converts Eu<sup>3+</sup> to Eu<sup>2+</sup> generating the Eu<sup>2+</sup> strong emission during irradiation? (2) Why does the intensity of the Eu<sup>2+</sup> emissions has a different behavior from the one observed for the Eu3+ emissions? In the following discussion, we show that both Eu<sup>3+</sup> and Eu<sup>2+</sup> are incorporated in the matrix at two Ba<sup>2+</sup> sites and, for Eu<sup>3+</sup>, the charge compensation mechanism is provided via interstitial oxygen (O<sub>i</sub>), as predicted in previous work.21

The presence of the characteristic emission of Eu<sup>2+</sup> and Eu<sup>3+</sup> in the XEOL spectra cannot be explained only by the existence of both ionic species in the material before irradiation with X-rays, as pointed out by the results in Fig. 1. The relative intensities of the Eu<sup>2+</sup> to the Eu<sup>3+</sup> luminescence bands are very different when the samples are excited with UV-visible light or X-rays. PL emission spectra excited with 245 nm (5.06 eV) photons exhibited only typical emissions due to the 4f → 4f transitions of Eu<sup>3+</sup> ions, as shown in previous work.<sup>21</sup> However, when the same samples were irradiated with X-rays, an intense emission band associated with Eu<sup>2+</sup> transitions and weak peaks associated with Eu<sup>3+</sup> were present, as shown in Fig. 1 and 2. The XAS spectrum, shown in Fig. 4, is another strong evidence for the presence of Eu<sup>2+</sup> in the sample. These results confirm that the X-rays induced the reduction of a part of Eu<sup>3+</sup> to Eu<sup>2+</sup>. Similar behavior was also observed for Eu-doped SrAl<sub>2</sub>O<sub>4</sub>.<sup>31</sup> This reduction process, however, is not stable after X-ray excitation, as observed in a previous work using dispersive X-ray absorption spectroscopy (DXAS).<sup>32</sup>

The main difference between the excitation with 245 nm (5.06 eV) light and X-ray photons is that the former produces only electronic transitions associated with the Eu<sup>3+</sup> centers while

the latter are able to excite deep core electrons to the conduction band (photoelectric process). As a consequence, the recovery to the ground state in both cases follows quite different routes. In the case of 245 nm excitation, the excited Eu<sup>3+</sup> centers decay via the well-known  $^5D_0 \rightarrow ^7F_j$  (j=0 to 4) transitions. The process is basically a "local" process involving rearrangements of the electronic distribution of the Eu<sup>3+</sup> ions.

The obvious mechanism that will recover the material to the ground state is the direct recombination of the electrons in the conduction band with the holes in the top of the valence band. This direct recombination can result in photons being emitted and these photons can be directly absorbed by the  $Eu^{3+}$  ions producing  $Eu^{3+}$  in the excited state that will decay to the ground state emitting the typical  $Eu^{3+}$  emission lines.

The above mechanism, however, does not explain the emission coming from  $\mathrm{Eu}^{2+}$  ions that dominates the emission spectra. But this is not the only possibility though. The electrons from the conduction band can also be captured by  $\mathrm{Eu}^{3+}$  ions creating  $\mathrm{Eu}^{2+}$  in the excited state that decay to the ground state producing the broad and dominant band at around 500 nm.

The local environment of the original Eu<sup>3+</sup> ions is not expected to be the same as the local symmetry of the Eu<sup>2+</sup> ion. The Eu<sup>3+</sup> substituting at the Ba site requires charge compensating defects, which is not the case for the Eu2+. Previous computer modeling results<sup>23</sup> revealed that the main charge compensating defect is  $O_i^{\prime\prime}$  (oxygen interstitial with an effective charge of -2) located near the Eu<sup>3+</sup>. So, the process that takes place in the material that reduces a great part of the Eu<sup>3+</sup> to Eu<sup>2+</sup> under X-ray irradiation also neutralizes the Oi accompanying defects. It is possible that the electrons generated after absorption of the X-rays are captured by Eu<sup>3+</sup> in the excited state, while the hole generates a  $V_k$ -type defect center, *i.e.*, an  $O_2^{\ 3-}$  molecule formed by a normal  $O^{2-}$  lattice anion and the  $O_i^{''}$  trapping the hole. Thus, Eu<sup>2+</sup> produced via X-rays will certainly have a different local symmetry as compared to the Eu<sup>2+</sup> incorporated during the production process of BaAl<sub>2</sub>O<sub>4</sub>. This model also explains the fact that Eu2+ is not stable after the irradiation process ceased because the V<sub>k</sub>-type defect center is not stable and the hole captured by the O<sub>i</sub>" needs to be neutralized by recombination with the electron captured by the neighboring Eu<sup>3+</sup>, recovering the original neutral state of the material before irradiation. This recombination process is more likely to occur via tunneling due to the proximity of the two sites in the crystalline matrix.

The luminescence emissions excited by X-rays are thus caused from excited states of  $Eu^{2+}$  and  $Eu^{3+}$  that are produced during irradiation, after the main core absorption has taken place. Let us consider first the case of the X-ray photons with energy close to the Ba  $L_{\rm III}$  absorption edge. After X-ray absorption by Ba ions, a cascade of processes is triggered by the presence of electrons in the conduction band (CB) and holes in the Ba core. In a first stage, both X-ray fluorescence and Auger processes occur, as follows: (i) electrons from M core shells fill the hole in the  $L_{\rm III}$  core shell releasing the typical  $L_{\alpha's}$  and  $L_{\beta's}$  X-ray fluorescence lines of Ba, (ii) the Auger process that involves a recombination of an M electron with the hole at the  $L_{\rm III}$  shell and the released energy is absorbed by another electron in the

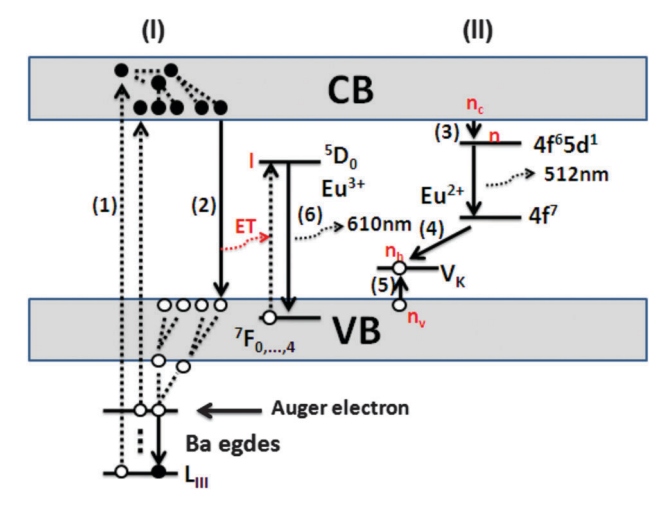


Fig. 7 XEOL mechanism in the BaAl<sub>2</sub>O<sub>4</sub>:Eu, excited at the Ba L<sub>III</sub> edge.

M shells that is ejected to the CB; this secondary electron leaves a second hole at the M levels of the Ba ions. Similar processes may be repeated several times until the holes created move up to the valence levels, close to the top of the valence band (VB). Then, the electrons from the CB decay to the bottom of the VB as described previously *via* multiple scattering by the ions or *via* electron–electron inelastic scattering.<sup>33</sup> Fig. 7 show a schematic representation of the process as described in stage (I).

Most of the electrons now in the bottom of the conduction band recombine with the holes in the top of the valence band, and some of this recombination will produce photons that can directly excite Eu<sup>2+</sup> and/or Eu<sup>3+</sup> ions. Excited Eu species decay to the ground state emitting the XEOL photons: Eu<sup>2+</sup> in the excited state decay from the 4f<sup>6</sup>5d<sup>1</sup> excited state configuration to the 4f<sup>7</sup> ( $^8\mathrm{S}_{7/2}$ ) ground state generating a broad emission band at around 500 nm, and Eu<sup>3+</sup>  $^5\mathrm{D}_0$  excited states decay to the ground states  $^7\mathrm{F}_{0\to 4}$  emitting the bands at around 600–700 nm. This is indicated by the ET shown as arrows in Fig. 7 and all Eu decay processes marked as stage II, also shown in Fig. 7.

An important issue here is that this model can not only explain the appearance of the Eu<sup>2+</sup> emission upon irradiation due to the Eu<sup>3+</sup> to Eu<sup>2+</sup> reduction, but can also account for the behavior of the emission intensities of both species as the energy of the incident photons increased. Some of the existing electrons in the conduction band are trapped in the Eu ion (accompanied by the hole being trapped in the Vk center, as discussed above), and that the trapping process will produce Eu<sup>2+</sup> in the excited state, as indicated by stage (II) in Fig. 7. This will produce Eu2+ in the excited state and should enhance the emission bands due to Eu<sup>2+</sup>, as observed before in Fig. 5. As the energy of the incident X-ray photons increased, the kinetic energy of the primary photoelectron increased too, increasing the probability of electron-electron inelastic scattering that, in turn, will increase the number of electrons in the conduction band. The increase in the concentration of electrons in the conduction band will increase the probability of the Eu3+ ions to trap electrons and reduce to Eu2+ producing, as a consequence, an increase of the emission due to the Eu<sup>2+</sup> ions, as observed in Fig. 5.

PCCP **Paper** 

All these processes are expected to cause a reduction in the emission of Eu<sup>3+</sup> since the number of trivalent species tends to decrease as the availability of electrons in the conduction band increase, as also observed in Fig. 6.

The XEOL spectrum is formed by Eu<sup>3+</sup> and Eu<sup>2+</sup> emissions that are produced during irradiation, after the photons are absorbed by the inner shells of the ions. Thus, the total XEOL efficiency  $\eta^{\tau}$  will have two terms, as follows:

$$\eta^{\tau}(E_{\text{incident}}) = \eta^{\text{Eu}^{2+}}(E_{\text{incident}}) + \eta^{\text{Eu}^{3+}}(E_{\text{incident}})$$
(1)

where  $\eta^{\text{Eu}^{2+}}$  and  $\eta^{\text{Eu}^{3+}}$  are the efficiency of the Eu<sup>2+</sup> and Eu<sup>3+</sup> luminescence centers, respectively. The scintillation efficiency for MeV photons has been described by Bizarri.<sup>34</sup> But for X-rays having energies of a few eVs to few hundreds of eV, the main process is the photoelectric effect that will depend strongly on the energy of the X-rays and the chemical elements of the material.

The XEOL process described in the present work is clearly produced by different contributions for the creation of the electron-hole pair that should be considered. The energy  $E_{e/h}$ needed to create an electron-hole pair depends not only on  $E_{\text{incident}}$ , as described in eqn (1), but should include all other processes that contribute to the creation of the electron-hole pair, such as the X-ray fluorescence and the Auger process. Furthermore, when electrons are promoted to the CB with a net kinetic energy there is a possibility that electron-electron inelastic scattering occurs increasing  $N_{e/h}$ . In order to include all processes, a new equation for the rate creation of electronhole pairs per volume  $\sigma_1$  is proposed as follows:

$$\sigma_1 \equiv N_{\rm e/h} = \mu(E_{\rm incicent})$$

$$\times \left[ 1P_{\rm Pe} + 2P_{\rm A} + \left( \frac{E_{\rm incident} - E_{\rm edge} + \beta E_{\rm g}}{\beta E_{\rm g}} \right) \right]$$
(2

where  $\mu(E_{\text{incident}})$  is the absorption coefficient of the material. The term within brackets accounts for the average number of electron-hole pairs formed per absorbed photon.  $P_{Pe}$  and  $P_{A}$ are the relative probabilities for X-ray fluorescence or Auger processes, respectively. Each absorbed photon that produces X-ray fluorescence emission generates one electron-hole pair. For the Auger process two electron-hole pairs are formed per absorbed photon. The relative probability between these two processes depends on the atomic number of the targeting element.<sup>35</sup> The third process that contributes to the formation of electron-hole pairs is the electron-electron inelastic scattering that is proposed to follow a simple energy ratio rule between the net kinetic energy of the electron promoted to the CB and the energy needed to generate one electron-hole pair that is considered to be  $\beta E_g$ . All these processes are represented in Fig. 7 as process (1).

The efficiency of the luminescence centers, in turn, will depend on the number of excited centers, the efficiency with which an energy carrier is going to excite a luminescence center and the quantum efficiency of the luminescence center, as follows:

$$\eta^{\mathrm{Eu}^{2+}}(E_{\mathrm{incident}}) = S^{\mathrm{Eu}^{2+}}Q^{\mathrm{Eu}^{2+}}n(E_{\mathrm{incident}})$$

and

$$\eta^{\text{Eu}^{3+}}(E_{\text{incident}}) = S^{\text{Eu}^{3+}}Q^{\text{Eu}^{3+}}l(E_{\text{incident}})$$
 (3)

where n and l stand for the concentration densities of Eu<sup>2+</sup> and Eu<sup>3+</sup> ions in excited states, respectively. As the concentrations of the luminescence center n and l change with the incident photon energy ( $E_{incident}$ ) the XEOL intensity due to each one of the luminescence centers changes.

In order to obtain the equilibrium values for n and l when the sample is excited around the Ba LIII edge, a set of rate equations for the electrons and the holes are required. The total process can be represented by a set of simultaneous differential equations that describe the traffic of charge carriers between: (i) the conduction and valence bands, (ii) charge traps and (iii) recombination centers. On deriving the equations, the following processes were taken into account:

- (1) The incident photons create electron-hole pairs via X-ray fluorescence, Auger and electron-electron inelastic scattering, as described by eqn (2);
- (2) Direct recombination of the electrons and holes that can excite Eu3+;
- (3) Electrons in the CB can be trapped in Eu<sup>3+</sup> traps, generating Eu<sup>2+</sup> in an excited state, which decays to the ground state producing the Eu<sup>2+</sup> characteristic luminescence;
- (4) Holes are trapped in Vk centers accompanying the electrons trapped in the Eu2+ centers;
- (5) Electrons from Eu<sup>2+</sup> and holes in V<sub>k</sub> centers recombine via tunneling, as discussed earlier;
- (6) Decay of the excited Eu<sup>3+</sup> from the excited states to the ground state producing the characteristic  ${}^5D_0 \rightarrow {}^7F_I Eu^{3+}$  emissions.

All these processes are marked in Fig. 7 according to the order quoted above. These can be related by a set of simultaneous differential equations which describe the traffic of charge carriers between conduction and valence bands, traps and recombination centers.

$$n_c + n = n_v + n_b \tag{4}$$

$$\frac{\mathrm{d}n_{\mathrm{c}}}{\mathrm{d}t} = \sigma_{1} - \sigma_{2}n_{\mathrm{c}}n_{\mathrm{v}} - \sigma_{3}n_{\mathrm{c}}(c - n - l) \tag{5}$$

$$\frac{\mathrm{d}n}{\mathrm{d}t} = \sigma_3 n_{\rm c} (c - n - l) - \sigma_4 n \left(\frac{c}{2} + n_{\rm h}\right) \tag{6}$$

$$\frac{\mathrm{d}l}{\mathrm{d}t} = \sigma_2 \tau n_{\rm c} n_{\rm v} (c - n - l) - \sigma_6 n_{\rm v} l \tag{7}$$

$$\frac{\mathrm{d}n_{\mathrm{h}}}{\mathrm{d}t} = \sigma_4 n_{\mathrm{v}} \left( \frac{c}{2 - n_{\mathrm{h}}} \right) - \sigma_3 n_{\mathrm{v}} n_{\mathrm{c}} \tag{8}$$

$$\frac{\mathrm{d}n_{\mathrm{v}}}{\mathrm{d}t} = \sigma_{1} - \sigma_{4}n_{\mathrm{h}}\left(\frac{c}{2} - n_{\mathrm{h}}\right) \tag{9}$$

where  $n_c$ , concentration of electrons in the conduction band;  $n_c$ concentration of electrons trapped in the excited state of  $Eu^{2+}$  (4f<sup>6</sup>5d<sup>1</sup>);  $n_h$ , concentration of holes trapped in  $V_k$ centers;  $n_{\nu}$ , concentration of holes in the valence band; l, concentration of electrons trapped in the excited state of Eu<sup>3+</sup>(4f<sup>7</sup>); **PCCP** Paper

c, concentration of Eu ions in the matrix;  $\sigma_1$ , creation rate of electron-hole pairs;  $\sigma_2$ , recombination probability of conduction band electrons and valence band holes;  $\sigma_3$ , trapping probability of conduction band electrons for the excited state of Eu<sup>2+</sup>;  $\sigma_4$ , recombination probability of conduction band electrons and V<sub>k</sub> centers;  $\sigma_5$ , recombination probability of the  $V_k$  center and the valence band;  $\sigma_6$ , recombination probability of the electron luminescence center (Eu<sup>3+</sup>) and the valence band;  $\tau$ , transference probability of energy of the electron-hole pair recombination for the excitation of Eu<sup>3+</sup>.

This system of 6 coupled differential eqn (4)-(9) can be simplified to just 3 equations using the charge carrier neutrality (eqn (4)) and the fact that  $n_h = n$  for any t. From eqn (4), this gives  $n_c = n_v$  and the new set of coupled equations are:

$$\frac{\mathrm{d}n_{\rm c}}{\mathrm{d}t} = \sigma_1 - \sigma_2 n_{\rm c}^2 - \sigma_3 n_{\rm c} (c - n - l) \tag{10}$$

$$\frac{\mathrm{d}n}{\mathrm{d}t} = \sigma_3 n_{\rm c} (c - n - l) - \sigma_4 n \left(\frac{c}{2} - n\right) \tag{11}$$

$$\frac{\mathrm{d}l}{\mathrm{d}t} = \sigma_2 \tau n_\mathrm{c}^2 (c - n - l) - \sigma_6 l n_\mathrm{c} \tag{12}$$

This is still a very complex system of differential equations that can be solved only numerically. The initial conditions are that at t = 0, i.e., before the X-ray beam hits the sample, the conduction band and the electron traps are empty. Also, the concentration of Eu<sup>3+</sup> centers in the excited state should be zero since in the model it is considered that the excitation occur via energy transfer from recombination of the electron-hole pairs.

One reasonable hypothesis is that irradiation time is always much greater than any of the characteristic times of the 6 processes involved in the XEOL emission. This is especially true for the results obtained in the present work where the average time between each of the measurements during the scanning of the X-ray photon energy is about 2-4 s. This means that the sample can be considered always under equilibrium conditions for each X-ray energy measured, corresponding to the solution of the equations for  $t \to \infty$ . If the system is considered to be in equilibrium, the following will apply:

$$n_c(0) = 0; n(0) = 0; l(0) = 0$$
 (13)

$$\frac{\mathrm{d}n_{\mathrm{c}}(\infty)}{\mathrm{d}t} = 0; \ \frac{\mathrm{d}n(\infty)}{\mathrm{d}t} = 0; \ \frac{\mathrm{d}l(\infty)}{\mathrm{d}t} = 0 \tag{14}$$

Thus, using eqn (13) and (14), the three differential equations can be simplified and reduced to their behavior when  $t_{\rightarrow \infty}$ giving:

$$0 = \sigma_1 - \sigma_2 n_c^2 - \sigma_3 n_c (c - n - l) \tag{15}$$

$$0 = \sigma_3 n_{\rm c}(c - n - l) - \sigma_4 n \left(\frac{c}{2} - 2\right) \tag{16}$$

$$0 = \sigma_2 \tau n_c^2 (c - n - l) - \sigma_6 l n_c$$
 (17)

This is now a system of coupled equations that in principle could be solved but one should consider a different approach.

Let us start by observing that the possibility of occurrence of each one of the processes described before is just given by a

probability constant associated with the particular process of interest times the equilibrium concentration of the available starting and ending levels for both electrons and holes. As an example, the direct electron-hole recombination is given by  $\sigma_2 n_{\rm c} n_{\nu}$ , where  $n_{\rm c}$  is the concentration of electrons in the CB,  $n_{\nu}$ is the concentration of holes in the VB and  $\sigma_2$  is the probability coefficient associated with this process (number 2 in Fig. 7). The trapping of electrons in the Eu<sup>2+</sup> ions is given by  $\sigma_3 n_c (c - n - l)$ . In this case, the probability needs to take into account the concentration of the "available" Eu2+ sites, which is given by the term (c - n - l), that is the difference between the total Eu<sup>3+</sup> in the matrix and the Eu<sup>3+</sup> either in an excited state or the Eu<sup>2+</sup> sites already occupied.

The alternative approach to directly solving eqn (15)-(17) is to recognize that there is a competition between the trapping of electrons in the Eu<sup>2+</sup> centers and the direct recombination with holes in a way that it is possible to write:

$$\sigma_3 n_c (c - n - l) = x \sigma_2 n_c^2 \tag{18}$$

with x being a weighting parameter. Using this assumption, the system of equations can be solved giving:

$$n_{\rm c} = \sqrt{\frac{\sigma_1}{\sigma_2(1+x)}}\tag{19}$$

$$l = \frac{(c-n)}{\left(\frac{1+\sigma_6}{\sigma_2 \tau n_c}\right)} \tag{20}$$

$$n = \frac{1}{2} - \frac{1}{2}\sqrt{1 - K}$$
 with  $K = \frac{8x\sigma_2 n_c^2}{c\sigma_4}$  (21)

In the other work, the number of electrons in the conduction band depends directly on the rate of creation of electron-hole pairs and inversely on the recombination of electrons in the CB with the VB.

The use of the weighting parameter x makes the solutions for  $n_c$ , n and l much easier to interpret in terms of the physical process involved in the XEOL emission. Eqn (19), as an example, shows that the equilibrium concentration of electrons in the CB (and consequently, the holes in the VB) will depend only on the ratio of the probability of the electron-hole pair creation, shown in Fig. 7 as process 1, to the direct electron-hole recombination (process 2) times the probability for trapping charges (process 3), represented by the x weighting parameter. Although this would be an expected result from the point of view of the physical phenomena involved here, the surprising thing is that the equilibrium concentration of electrons in the CB depends on the square root of this ratio. Another interesting feature is that all three concentrations  $n_c$ , n and l will depend on the energy of the incident photons, via  $\sigma_1$ . This is an important feature that will allow the interpretation of the XEOL results as a function of the incident photon energy.

Knowing the equilibrium concentration, n and l, as a function of the incident photon energy, it should be possible, in principle, to evaluate the luminescence efficiency of both Eu<sup>2+</sup> and Eu<sup>3+</sup> centers, provided that the quantum efficiencies of the luminescence Paper PCCP

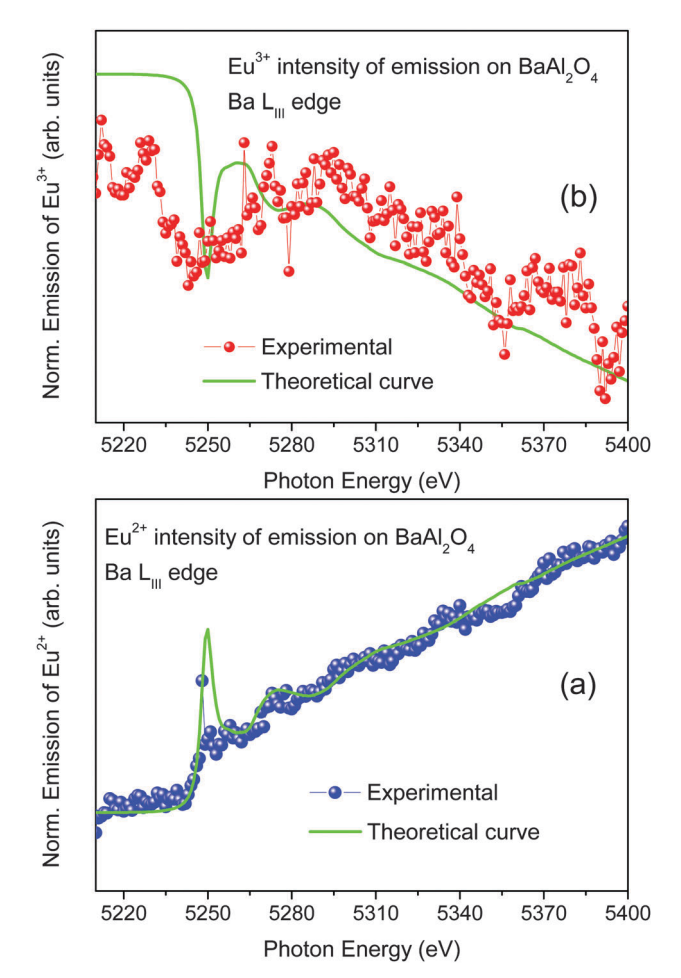


Fig. 8 Comparison between the luminescence intensity when the sample is excited at the Ba  $L_{III}$  edge. (a) Intensity of  $Eu^{2+}$  and (b) intensity of  $Eu^{3+}$ .

centers are known. However, one should also stress that the parameters involved in the above equations are not easily accessible and most of them are rather difficult to evaluate. One possible solution for that is *via* numerical simulation where a sensible choice of parameters may be done and a few can be varied producing numerical curves that could be compared to experimental results. That was the strategy used in the present work.

*Via* a trial-and-error approach repeated many times, examples of such simulated curves can be seen in Fig. 8(a) and (b). The "theoretical curves" were obtained using the following parameters:  $\sigma_2 = \sigma_3 = \sigma_4 = \sigma_5 = \sigma_6 = 0.1$ ,  $\mu = \text{normalized}$  experimental absorption, as obtained *via* the usual EXAFS measurement, PPE = 0.2, PA = 0.8,  $\beta = 2$ ,  $E_g = 6.5$  eV and  $x = 10^{-6}$ . For this set of parameters, it is interesting to show that the XEOL contribution from Eu<sup>2+</sup> gives a direct absorption edge, as compared to the usual EXAFS measurement, as shown in Fig. 8(a), while the Eu<sup>3+</sup> XEOL emission is predicted to give an "inverted" absorption edge, as shown in Fig. 8(b). The qualitative agreement is reasonably good, considering that there are a number of parameters that were not possible to obtain.

Two final comments should be made. One is regarding the meaning of the weighting parameter *x* and its role in defining

the direction of the edge jump. The value  $x=10^{-6}$  was the one that could reproduce both behavior for the Eu<sup>3+</sup> and Eu<sup>2+</sup> XEOL emission spectra, meaning that the trapping process that produces Eu<sup>2+</sup> in the excited state is much more likely to occur than the direct electron–hole recombination. The second comment is that at the present stage of the model it is not possible to obtain XEOL simulated curves with intensities directly comparable to the experimental XEOL curves and this means that the "theoretical curves" must be viewed as a general trend that, nevertheless, reproduces quite well the experimental trend and shape, giving enough interesting results that can be used to further interpret XEOL emission spectra for a variety of materials.

### 5 Conclusions

The XEOL emission and excitation spectra of Eu-doped  $BaAl_2O_4$  samples were studied in detail in the present paper. Samples were prepared as nanopowders and their excitation spectra were recorded in the X-ray energy range around the Ba and Eu  $L_{\rm III}$  absorption edges, from 5200 to 5500 eV and from 6900 to 7100 eV, respectively.

A model was built to explain the facts that the intensity of XEOL emission due to Eu<sup>2+</sup> increased and the one due to the Eu3+ species decreased as the energy of the X-ray photons increased. The following 6 processes were considered to take place during X-ray exposure: (1) the incident photons create electron-hole pairs in the conduction and the valence bands (CB and VB), respectively, via X-ray fluorescence, the Auger process and electron-electron inelastic scattering; (2) direct recombination of the electron-hole pairs release photons that are able to excite the Eu<sup>3+</sup> ions; (3) electrons in the CB can be trapped by Eu3+ ions, generating Eu2+ in excited states that decays to the ground state producing the Eu2+ characteristic luminescence; (4) holes are trapped in V<sub>k</sub>-type centers accompanying the electrons trapped in the Eu<sup>2+</sup> centers; (5) electrons from Eu<sup>2+</sup> and holes in Vk centers recombine via tunneling, recovering the Eu<sup>3+</sup> and the O<sub>i</sub> defects initially present in the material; and (6) the decay of the excited Eu3+ from the excited states to the ground state produces the characteristic <sup>5</sup>D<sub>0</sub> to <sup>7</sup>F<sub>I</sub> Eu<sup>3+</sup> emissions. All these processes were mathematically represented by a set of 6 coupled differential equations where the variables of interest are the concentration of the electrons in the conduction band, the concentration of holes in the valence band and the concentrations of the Eu3+ and Eu2+ species in the excited states, the last two of them being directly associated with the Eu3+ or Eu2+ emission intensities. All these concentrations are considered to be functions of both exposure time and incident X-ray photon energy.

Two main approximations were done to extract the behavior of both emission intensities as functions of the X-ray photon energy: (1) the exposure time is long enough that the registered emissions in the experiments are due to the equilibrium concentration and (2) the competition between the direct electronhole pair recombination and the electron trapped at  $Eu^{2+}$  accompanied by the hole being trapped in  $V_k$  defect centers can be represented by a weighting factor. These two approximations

reduce the set of differential equations to a system of coupled equations for which the solutions could be found. These solutions gave the behavior of the concentrations of interest as functions of the photon energy, but they also depend on a number of parameters connected to each one of the 6 processes described above.

Mathematical simulations of the solutions using a set of reasonable values for the parameters were proved to be able to reproduce reasonably well the experimental partial XEOL excitation spectra due to each one of the Eu species.

The main conclusion that could be drawn is that by considering possible processes that happen during X-ray energy absorption, charge carrier generation and trapping and the possible recombination pathways to recover the initial state of the material it is possible to explain quite well an apparently complicated X-ray excitation spectra behavior in Eu-doped BaAl<sub>2</sub>O<sub>4</sub>. In summary, the proposed mechanism provides a fundamental understanding regarding the characteristic XEOL emission of the Eu-doped BaAl<sub>2</sub>O<sub>4</sub> and there is no reason why a similar approach could be applied to a range of other materials that present any possible XEOL emission response.

## Acknowledgements

The authors are grateful to FINEP, CAPES and CNPq (No. 470.972/2013-0). Synchrotron radiation measurements were done at LNLS-Brazilian Light Synchrotron Laboratory/CNPEM/MCT under proposal No. XAFS-13512/12.

#### References

- 1 M. Weber, Nucl. Instrum. Methods Phys. Res., Sect. A, 2004, 527, 9-14.
- 2 V. Mikhailik, H. Kraus, J. Imber and D. Wahl, *Nucl. Instrum. Methods Phys. Res., Sect. A*, 2006, **566**, 522–525.
- 3 M. D. Birowosuto, P. Dorenbos, C. W. E. van Eijk, K. W. Krämer and H. U. Güdel, *J. Phys.: Condens. Matter*, 2006, **18**, 6133.
- 4 B. Shul'gin, S. Buzmakova, L. Viktorov, A. Krymov, V. Petrov, S. Podurovskii, A. Kozlov, B. Shapiro, M. Shrom, A. Nepomnyashchikh, P. Figura and V. Lakhov, *At. Energy*, 1993, 75, 534–538.
- 5 S. Neicheva, A. Gektin, N. Shiran, K. Shimamura and E. Villora, *Radiat. Meas.*, 2007, **42**, 811–814.
- 6 Y. Zorenko, V. Gorbenko, I. Konstankevych, T. Voznjak, V. Savchyn, M. Nikl, J. Mares, K. Nejezchleb, V. Mikhailin, V. Kolobanov and D. Spassky, *Radiat. Meas.*, 2007, 42, 528–532.
- 7 H.-M. Lee, C.-C. Cheng and C.-Y. Huang, *Mater. Res. Bull.*, 2009, 44, 1081–1085.

- 8 J. A. Mares, A. Beitlerova, M. Nikl, N. Solovieva, C. D'Ambrosio, K. Blazek, P. Maly, K. Nejezchleb and F. de Notaristefani, *Radiat. Meas.*, 2004, **38**, 353–357.
- 9 P. Montes, M. Valerio and M. S. Rezende, *J. Electron Spectrosc. Relat. Phenom.*, 2013, **189**, 39–44.
- 10 R. Sakai, T. Katsumata, S. Komuro and T. Morikawa, *J. Lumin.*, 1999, **85**, 149–154.
- 11 D. Qiu and W.-Z. Zhang, Acta Mater., 2007, 55, 6754-6764.
- 12 D. Jia, X. jun Wang, E. van der Kolk and W. Yen, *Opt. Commun.*, 2002, **204**, 247–251.
- 13 Z. Lou, J. Hao and M. Cocivera, J. Phys. D: Appl. Phys., 2002, 35, 2841.
- 14 G. Agostini and C. Lamberti, Characterization of semiconductor heterostructures and nanostructures, Elsevier, 2011.
- 15 M. Macedo and J. Sasaki, Produção de Pós Nanoparticulados, INPI 0203876-5, 2002.
- 16 A. Bianconi, D. Jackson and K. Monahan, *Phys. Rev. B: Condens. Matter Mater. Phys.*, 1978, 17, 2021–2024.
- 17 J. Goulon, P. Tola, M. Lemonnier and J. Dexpert-Ghys, *Chem. Phys.*, 1983, 78, 347–356.
- 18 A. Belsky, P. Chevallier, E. Mel'chakov, C. Pédrini, P. Rodnyi and A. Vasil'ev, *Chem. Phys. Lett.*, 1997, **278**, 369–372.
- 19 S. Emura and S. Masunaga, Phys. Rev. B: Condens. Matter Mater. Phys., 1994, 49, 849–853.
- 20 B. dos Santos Jr., R. Araujo, M. Valerio and M. dos S. Rezende, *Solid State Sci.*, 2015, 42, 45–51.
- 21 M. dos S. Rezende, C. Arrouvel, S. Parker, J. Rey and M. Valerio, *Mater. Chem. Phys.*, 2012, **136**, 1052–1059.
- 22 M. S. Rezende, P. J. Montes, M. E. Valerio and R. A. Jackson, *Opt. Mater.*, 2012, **34**, 1434–1439.
- 23 M. V. dos S. Rezende, M. E. Valerio and R. A. Jackson, *Opt. Mater.*, 2011, 34, 109–118.
- 24 R. D. Shannon, J. Appl. Phys., 1993, 73, 348-366.
- 25 Y. Lin, Z. Zhang, Z. Tang, J. Zhang, Z. Zheng and X. Lu, Mater. Chem. Phys., 2001, 70, 156–159.
- 26 F. C. Palilla and A. K. Levine, Appl. Opt., 1966, 5, 1467-1468.
- 27 G. Blasse, J. Solid State Chem., 1986, 62, 207-211.
- 28 M. Peng and G. Hong, J. Lumin., 2007, 127, 735-740.
- 29 G. Gasparotto, S. Lima, M. Davolos, J. Varela, E. Longo and M. Zaghete, *J. Lumin.*, 2008, **128**, 1606–1610.
- 30 P. J. Montes, M. E. Valerio and G. de M. Azevedo, *Nucl. Instrum. Methods Phys. Res., Sect. B*, 2008, **266**, 2923–2927.
- 31 P. J. R. Montes and M. E. G. Valerio, *J. Lumin.*, 2010, **130**, 1525–1530.
- 32 M. V. dos S. Rezende, M. E. G. Valerio and R. A. Jackson, *Mater. Res. Bull.*, 2015, **61**, 348-351.
- 33 C. Pédrini, Phys. Solid State, 2005, 47, 1406-1411.
- 34 G. Bizarri, J. Cryst. Growth, 2010, 312, 1213-1215.
- 35 D. Attwood, *Soft X-rays and extreme ultraviolet radiation: principles and applications*, Cambridge University Press, 1999.